Temperature Dependence of the Band-Gap Energy and Sub-Band-Gap Absorption Tails in Strongly Quantized ZnSe Nanocrystals Deposited as Thin Films

ARTICLE *in* THE JOURNAL OF PHYSICAL CHEMISTRY C · SEPTEMBER 2010

Impact Factor: 4.77 · DOI: 10.1021/jp102773z

3 AUTHORS:

Biljana Pejova
Ss. Cyril and Methodius University
52 PUBLICATIONS **957** CITATIONS
SEE PROFILE

B. Abay
Ataturk University
42 PUBLICATIONS **638** CITATIONS
SEE PROFILE

Irina Bineva
Bulgarian Academy of Sciences
44 PUBLICATIONS **292** CITATIONS
SEE PROFILE

Temperature Dependence of the Band-Gap Energy and Sub-Band-Gap Absorption Tails in Strongly Quantized ZnSe Nanocrystals Deposited as Thin Films

Biljana Pejova,*,† Bahattin Abay,‡ and Irina Bineva§

Institute of Chemistry, Faculty of Natural Sciences and Mathematics, Sts. Cyril and Methodius University, POB 162, 1001 Skopje, Macedonia, Atatürk Üniversitesi, Fen-Edebiyat Fakültesi, Fizik Bölümü, 25240, Erzurum, Turkey, and Institute of Solid State Physics, Bulgarian Academy of Sciences, 72 Tzarigradsko Chaussee Blvd., 1784 Sofia, Bulgaria

Received: March 27, 2010; Revised Manuscript Received: July 3, 2010

The temperature-dependent optical absorption of 3D arrays of close-packed strongly quantized ZnSe QDs, deposited in thin film form, is studied in the interval from 11 to 340 K. Because of the particle size distribution and interdot coupling between proximal QDs within the QD arrays, the excitonic peaks are not visible at all, even at temperatures as low as 11 K. The temperature coefficient of the band-gap energy in the strongly quantized QD arrays was found to be twice larger than the value characteristic of a bulk ZnSe specimen. The Debye temperature, on the other hand, is shown to decrease by about 15% in comparison with the bulk value, which is attributed to the phonon confinement effects. It is shown that the sub-band-gap exponential absorption tails in the strongly quantized 3D QD arrays obey the Urbach−Martienssen rule. The temperature dependence of the Urbach energy and the relation between this quantity and the band-gap energy of the films could be excellently fitted to the predictions of the Cody's model. However, in contrast to the macrocrystalline semiconductors, the temperature-dependent component of the Urbach energy accounts for less than 15% of the overall value, which is attributed to the very high degree of inherent structural disorder in the QD arrays. This is in line with the conclusions derived from analyses of the temperature dependence of the steepness parameter, σ, which imply a rather high energy of the phonons contributing to the Urbach−Martienssen tails in the optical absorption of the QD arrays.

1. Introduction

Low-dimensional semiconductors have achieved a status of materials that have a crucial role in contemporary science and technology. This status arose from the remarkable size-dependent optical and electronic structure properties that these systems exhibit.[1−8] One of the most notable between these properties is the size-induced band-gap variation. It enables spectral tunability of light absorption and emission and enhancement of the oscillator strength of the transitions induced due to quantum confinement effects. Therefore, besides the fundamental importance that nanosized materials have in certain areas of physical chemistry, the new physics of low-dimensional semiconductors also allows for their wide application in optoelectronics and nonlinear optical devices. An abrupt and profound change of low-dimensional semiconductors' properties occurs when the "characteristic length" of nanoparticles becomes comparable to the exitonic Bohr radius[1−8] for the corresponding bulk material. The last quantity is a natural measure of the confinement length in semiconductors. To emphasize the quantum character of the confinement effects, along with the nanodimensions of a particle's characteristic length, the term "quantum dot" (QD) has been coined.[1−8] Systems composed of individual or diluted semiconductor QDs have been explored in detail, and their basic optoelectronic properties have been understood at a sufficient level of sophistication, at least in a qualitative sense.[1−8] However, in cases when individual QDs are close-packed (e.g., forming a *three-dimensional assembly* or *array* of QDs), further new opportunities are opened and fundamentally new aspects could be investigated. Studies of 3D arrays of QDs have allowed the collective physical phenomena, which develop upon interaction of the proximal QDs, to be explored. On the other hand, certain properties that are characteristic of individual QDs are retained (refs 9−16 and references therein). To emphasize that these superstructures correspond to a new form of organization of matter, the terms "*QD solid*" or "*colloidal crystal*" have been used, referring to 3D QD arrays in some recent publications devoted to this subject.[9−16]

Investigations of the fundamental absorption edge in semiconductors can provide extensive information concerning the band structures of crystals, the existence of excitons and their role in the mechanism of light absorption, the character of electron/exciton−phonon interactions, etc. Although the absorption edge is often quantitatively characterized by a single numerical parameter—the band-gap energy value—it could be characterized in a much more complete manner.

It has been recognized for the first time by Urbach[17] and Martienssen[18] that the absorption in silver halides and alkali halides does not occur sharply, but rather a sub-band-gap absorption tail of an exponential type is usually developed of the following form:

$$\alpha(h\nu, T) \sim \exp\left(\frac{h\nu - E_0}{E_U(T, X)}\right); \quad h\nu < E_g \tag{1}$$

In eq 1, $h\nu$ is the incident photon energy and E_0 roughly coincides with the energy of the lowest free exciton state at

* To whom correspondence should be addressed. Tel: +389-2-3117-055. Fax: +389-2-3226-865. E-mail: biljana@iunona.pmf.ukim.edu.mk.
† Sts. Cyril and Methodius University.
‡ Atatürk Üniversitesi.
§ Bulgarian Academy of Sciences.

10.1021/jp102773z
Published on Web 08/23/2010

zero lattice temperature, whereas E_U is the parameter determining the steepness of the Urbach tail (the Urbach energy). As introduced by Cody and co-workers,[19] parameter X appearing in eq 1 is a measure of the degree of structural disorder of the material. Such absorption tails are known as Urbach−Martienssen (UM) tails, and a number of possible explanations for their origin have been proposed in the literature. We will address some of these later in this paper, in the context of analysis of our experimental data. Equation 1 is, in fact, a mathematical formulation of the Urbach−Martienssen rule.[5,20−22] This kind of sub-band-gap exponential absorption behavior is actually of a quite universal nature in semiconductors.[20] It is generally thought that it could be due to excitonic smearing of the absorption edge at relatively higher temperatures (in comparison to those temperatures at which excitonic absorption bands are observed). The importance of the concept of excitons as electron−hole bound states is especially emphasized in the case of nanocrystalline semiconductors, with sizes in the several nanometers range.[5,23,24] Because the electrons and holes are confined to a small space region, the Coulomb interaction between them is much more pronounced in the case of three-dimensionally confined nanostructures in comparison with the bulk counterparts.

Ever since the statement of the Urbach rule for optical absorption of silver halides[17] (indirect band-gap materials) and its further establishing by Martienssen in the case of alkali halides[18] (direct band-gap materials), the temperature dependence of the UM absorption tails (along with the temperature dependence of E_g), has been studied for a number of systems (refs 25−33 and references therein). Also, many other aspects of the sub-band-gap exponential absorption have been addressed. These included the influence of external electric fields on the Urbach energy in the case of single crystals,[34] the influence of technological conditions of preparation of various single crystals (and also of the temperature and pressure) on the corresponding Urbach parameters,[35−42] the influence of hydrostatic pressure on the Urbach energy in the case of layered metal iodide crystals,[43] etc. Also, comparative studies of the Urbach and exciton absorption in the case of undoped and doped metal chalcogenide compounds (such as GaSe and Ga-doped GaSe as well as InSe and Er-doped InSe)[27−33] at various temperatures have been performed. The doping, hydrogenation, and post-deposition annealing influences on the optical absorption edge of various amorphous materials have been studied as well.[44−53] It is, however, of certain importance for both the fundamental physical chemistry and materials science and the potential applications of the semiconductor QD thin films to follow the evolution of these absorption tails upon controlled particle size reduction as well. It is exactly this aspect of semiconducting nanocrystalline materials that the present paper is devoted to.

Though, as could be concluded from the literature retrospective given above, the UM tails have been investigated in a number of semiconductor single crystals, and also in some thin films constituted by macrocrystalline and amorphous materials, it seems that considerably less attention has been devoted to their appearance in the optical absorption spectra of 3D assemblies of QDs. Investigations concerning this issue enable a number of further fundamental physical insights into the properties of QD assemblies to be obtained and also to gain some relevant implications for their potential applicability.

Continuing our work in the field of low-dimensional semiconductor materials (refs 54−67 and references therein), in the present paper, we study the temperature dependence of optical absorption in the case of 3D assemblies of strongly quantized ZnSe QDs, deposited in thin film form by our recently developed chemical deposition method,[64] which is similar to the one presented in ref 68, but with certain modifications that affected the thin film properties. The range from cryogenic temperatures (11 K) to about 350 K has been covered, putting a special emphasis on the temperature dependence of the band gap and Urbach energy.

Our interest for the title semiconductor compound arose due to the following facts that make it a rather attractive optoelectronic material. Zinc selenide has a rather wide band-gap energy; it is much transparent over a wide range of the visible spectrum and has a relatively large nonlinear optical coefficient.[69] Thin films of ZnSe are of importance in the fabrication of devices in the blue or ultraviolet region, devices useful in communication systems, electroluminescent structures compatible with large-area displays, and integrated circuits.[70,71] Recently, ZnSe thin films have been increasingly used in the preparation of high-efficiency solar cells based on environmentally friendly Cd-free thin films, such as $CuInS_2$, $CuInSe_2$, or $CuInGaSe_2$.[72,73] As zinc selenide crystallizes in two polymorphic modifications (cubic and hexagonal), it has been shown to be a very difficult task to synthesize thin films of this material that would consist of only a single phase (especially the cubic one) (ref 64 and references therein). Therefore, deeper fundamental analyses of the optical properties characteristic for the cubic phase 3D QD assemblies have been in a sense hampered. However, our recently developed chemical method enables deposition of 3D assemblies of strongly quantized QDs of cubic ZnSe, with a high crystallographic (phase) purity.[64] This method enabled such more in-depth studies to be performed for 3D assemblies constituted of QDs of only the cubic ZnSe polymorph.

2. Experimental Details

2.1. Preparation of the Substrates and Deposition of ZnSe Quantum Dots in Thin Film Form. Thin films composed of zinc selenide quantum dots (i.e., strongly quantized close-packed nanocrystals) were deposited onto standard microscope glasses using the chemical deposition method.[64] To provide better adhesion between the films and the substrates, prior to the deposition process, the later were treated in a diluted solution of tin(II) chloride and then annealed at 200 °C for about 20 min. During this treatment, small and stochastically distributed crystals of tin(II) oxide were created onto the glass surface, which, afterward, initiated heterogeneous nucleation and improved the film adhesion.[74]

Zinc selenide quantum dots were deposited chemically using sodium selenosulfate as a chalcogenide-releasing agent. The film growth solution was prepared from analytical-grade reagents (zinc sulfate or zinc acetate, sodium hydroxide, and 80% hydrazine hydrate), whereas the precursor of selenide ions was previously synthesized by adding gray selenium to a hot solution of sodium sulfite, stirring this mixture for 1 h at 90 °C and filtering the excess of gray selenium.[64] The solution of sodium selenosulfate is relatively unstable. Because of this, it was prepared prior to the thin film deposition process and kept in a dark container.

Glass substrates, previously treated as explained before, were placed in a beaker containing the growth solution prepared according to the procedure explained in more detail elsewhere.[64] The thin film deposition process was carried out for 1 h at about 60 °C. The terminal film thickness was about 300 nm. More details concerning the chemistry of the synthetic route have been presented in our previous papers dealing with the development of the synthetic route to this system.[63,64]

2.2. Structural Characterization and Investigation of Optoelectronic Properties at Various Temperatures. To identify the chemical composition of deposited materials in thin film form (and also in the form of precipitates) and also to determine the structure, average crystal size, lattice strain, and dislocation density, the X-ray diffraction method (XRD) for polycrystalline samples with monochromatic Cu Kα radiation was used. The diffractograms were recorded on a Philips PW 1710 diffractometer. The Debye−Scherrer approach was used for estimation of the average crystal size of the synthesized thin films and precipitates on the basis of recorded XRD patterns.

To investigate the optical properties of thin films composed of close-packed ZnSe quantum dots, their optical absorption spectra were recorded in the spectral range from 190 to 1100 nm on a PerkinElmer Lambda 2S UV−vis-NIR spectrophotometer in the temperature interval from 10 to 340 K. A Leybold-Heraeus cryogenic system was used, employing a closed liquid He system for low-temperature measurements. Sample temperatures were controlled with a precision of ±0.2 K employing a computer-controlled Leybold-Heraeus Variotemp HR1 temperature regulation system. Analysis and processing of the spectra was performed using the MS EXCEL and MICROCAL ORIGIN software packages.[75,76]

The thicknesses of ZnSe quantum dot thin films, required to convert the spectral dependence of the transmission coefficient $T(h\nu)$ to the spectral dependence of the absorption coefficient $\alpha(h\nu)$, were determined gravimetrically or interferometrically. Within the interferometric approach, the film thickness was calculated on the basis of recorded transmission spectra of investigated samples, using the following equation

$$d = \frac{1}{2}\frac{\lambda_1\lambda_2}{n(\lambda_1)\lambda_2 - n(\lambda_2)\lambda_1} \quad (2)$$

where λ_1 and λ_2 are wavelengths of the first and second interference maxima, whereas $n(\lambda_1)$ and $n(\lambda_2)$ are refractive indexes at λ_1 and λ_2, correspondingly. The values of $n(\lambda_1)$ and $n(\lambda_2)$ are taken from the graphical dependencies of n versus λ given in ref 77.

Coherent light-scattering experiments were performed in order to study the mechanism of zinc selenide crystal growth.[78]

The surface morphology of the layers was investigated by AFM measurements that were carried out using a Multimode V (Veeco, Santa Barbara, CA). Imaging was performed in tapping mode, and height, amplitude, and phase images were recorded. The scan rate was in the range of 1.5−2 Hz, and the images' resolution was 512 lines per scan direction. At least two different points on the sample surface were explored. Silicon cantilevers with a supersharp spike tip (TESP-SS, Veecoprobes) were used in the experiments. TESP-SS probes have a nominal resonance frequency of 320 kHz and a typical force constant of 42 N/m. The tip radius for these probes is in the range of 2−5 nm. Images were just flattened, and no further processing was performed.

3. Results and Discussion

3.1. Structural Properties of ZnSe Nanocrystalline QD Films. The Debye−Scherrer approach, based on the X-ray line broadening, was applied for an estimation of the average crystal size in the synthesized QD solids, using the Debye−Scherrer equation

$$D = \frac{4}{3}\frac{0.9\cdot\lambda}{\beta\cdot\cos\theta} \quad (3)$$

in which D is the average diameter of the crystals (in spherical approximation), λ is the wavelength of the used X-ray radiation, β is the full width at half-maximum intensity of the peak, and θ is the angle corresponding to the diffraction maximum.[79] In a manner explained in detail in our previous studies,[54,55,59,60] we have here also analyzed the influence of instrumental broadening of diffraction peaks on the actual crystal size calculated by the Debye−Scherrer equation. We have, however, found that neglect of the instrumental broadening leads to relative errors in the calculated average crystal radii of less than 1%.

According to the results obtained from XRD study, when zinc sulfate is used as a source of Zn^{2+} ions, the deposited material in thin film form (as well as the precipitate) is the pure cubic modification of zinc selenide with a sphalerite type of structure and a bulk unit cell parameter of 5.667 Å.[80] The X-ray diffractograms for the as-deposited and thermally treated ZnSe thin films and precipitates are given in Figure 1. The average crystal radius in the case of as-deposited ZnSe thin films estimated according to the Debye−Scherrer formula is 1.4 nm and is identical to the average crystal size for the corresponding precipitate. This is additional evidence for the colloidal (i.e., cluster) mechanism of crystal growth during the thin film deposition process, as was previously concluded on the basis of light-scattering experiments. In this context, it is worth noting that, in our recent studies, we have found out that the average crystal sizes of nanocrystalline semiconductor films determined by the Debye−Scherrer approach are in very good agreement with the values determined from the atomic force microscopy (AFM) studies.[55,56] ZnSe thin films, synthesized from this reaction system, do not undergo a change in chemical composition or crystal structure upon thermal treatments at 200 and 250 °C, irrespective on the duration of this treatment. However, the average crystal radius of the deposited material increases to 1.8 and 2.0 nm upon annealing at 200 and 250 °C, respectively. This average crystal size increase is due to coalescence and crystal growth upon annealing treatments. On the basis of these findings regarding the average crystal sizes, the deposited material may be classified as a three-dimensional array of ZnSe quantum dots (three-dimensionally confined nanostructures) in thin film form. However, this conclusion is supported by the value of the Bohr excitonic radius for bulk ZnSe (discussed later in the article), and it is also in line with the optical properties of the as-deposited and thermally treated thin film material.[63,64] When zinc acetate is used as a source of Zn^{2+} ions, the synthesized material also belongs to the cubic modification of zinc selenide with a nanocrystalline character. The average crystal radius in this case is 1.8 nm (again, this value being equal to the average crystal size of the precipitate, in line with the cluster mechanism of crystal growth). Upon annealing for about 1 h at 200 °C, the average crystal radius of these films increases to 2.2 nm. However, contrary to the case of ZnSe films deposited from $ZnSO_4$-containing growth solutions, in this case, upon prolonged thermal treatment of the films at 250 °C, impurities of ZnO were registered to appear. For the purpose of the present paper, our attention has been focused on as-deposited ZnSe films from the reactor containing zinc sulfate as a cation-releasing agent, which are characterized by most pronounced size quantization effects (i.e., a most pronounced band-gap energy blue shift with respect to the macrocrystalline value).

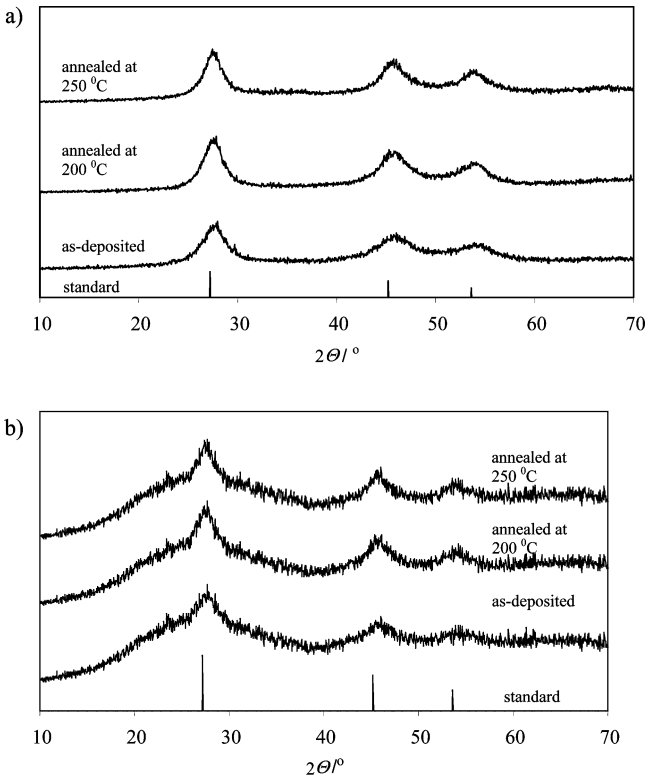

Figure 1. Recorded X-ray diffractograms for the as-deposited and thermally treated ZnSe precipitates (a) and thin films (b) obtained from the growth solution containing $ZnSO_4$ as a source of Zn^{2+} ions.

The refinement of unit cell parameters in the synthesized QD solids was done on the basis of the expression that arises from a combination of Brag's diffraction law and the equation that connects the interplanar distances d_{hkl} with the unit cell parameter in the case of the cubic crystalline system (to which the studied semiconductor belongs), in a manner described in our previous publications.[81] Also, the isotropic average lattice strain defined as[23]

$$\langle \varepsilon \rangle = \frac{|\Delta a|}{a_{\text{bulk}}} \tag{4}$$

or, alternatively, as[82]

$$\Delta\theta_{hkl} = -\varepsilon \cdot \tan(\theta_{hkl}) \tag{5}$$

(with subsequent averaging over all relevant peaks in the X-ray diffractograms) was calculated for both the as-deposited and the thermally treated ZnSe quantum dot thin films. The ε values computed by both approaches were found to be in excellent agreement. All of these parameters relevant to the present study are given in Table 1, together with the relevant optical spectroscopy data obtained at room temperature. Briefly, it could be concluded from Table 1 that the lattice constants (a) in the case of both as-deposited and thermally treated ZnSe quantum dots deposited in thin film form are notably smaller than the corresponding bulk literature values and, in both cases, they converge to the bulk value upon thermal annealing. These trends are obviously accompanied with lattice strain relaxation and a dislocation density decrease upon thermal annealing.

All these parameters in a sense characterize the degree of structural disorder in the chemically synthesized ZnSe QDs in thin film form. We will, therefore, use all of them as measures of the degree of structural disorder when interpreting the findings related to the Urbach−Martienssen absorption tails in the optical spectra of these variable-sized 3D quantum dots in thin film form. In this paper, however, we put the main emphasis on the temperature variation of absorption spectra in the case of as-deposited ZnSe nanocrystalline films, that is, those in which the size quantization effects are the most prominent. To the best of our knowledge, this is the first experimental study devoted to the temperature dependence of the band-gap energy of thin films composed of semiconductor quantum dots in the range from cryogenic to room temperatures, notably when the nanocrystalline films exhibit strongly pronounced quantum size effects.

TABLE 1: Basic Structural Parameters of As-Deposited and Thermally Annealed ZnSe Thin Films Synthesized Using Zinc Sulfate as a Zn^{2+} Ion Precursor Derived on the Basis of XRD Data[a]

	$\langle a \rangle$/Å	$\langle R \rangle$/nm	δ/nm^{-2}	$\langle \varepsilon \rangle$	E_g/eV
as-deposited	5.5885	1.4	0.13	0.0139	3.10
annealed at 150 °C	5.5893	1.5	0.11	0.0125	3.00
annealed at 200 °C	5.6033	1.8	0.08	0.0112	2.90
annealed at 250 °C	5.6054	2.0	0.06	0.0109	2.60

[a] See text for details.

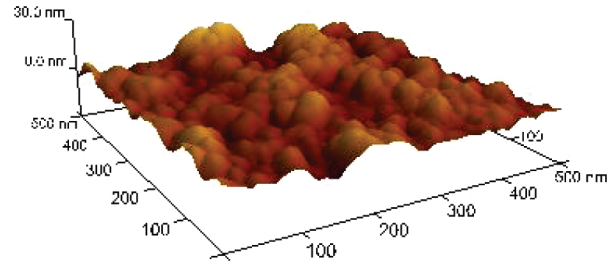

Figure 2. Three-dimensional surface AFM image of an as-deposited ZnSe thin film.

To further characterize the surface morphology of the as-deposited ZnSe films, as well as to provide a further proof of the conclusions drawn on the basis of the X-ray diffraction data, we have undertaken an AFM study. In Figure 2, a 3D AFM image of a typical thin film sample is shown. It is evident that the films are continuous and exhibit a pronounced nanocrystalline structure.

3.2. Optical Absorption Spectra of Nanocrystalline Films and the Temperature Dependence of the Band-Gap Energy. Optical properties of close-packed ZnSe nanocrystals deposited in the form of thin films were investigated by variable-temperature absorption spectroscopy. The measured spectral dependencies of transmission and reflection coefficients were used for construction of the spectral dependence of the absorption coefficient. If reflection phenomena are completely neglected, in the course of these analyses, the following relation between the two mentioned coefficients was employed:

$$\alpha(h\nu) = \frac{1}{d} \ln \frac{I_0(h\nu)}{I(h\nu)} = \frac{1}{d} \ln \frac{1}{T(h\nu)} \tag{6}$$

In the last equation, $h\nu$ is the energy of incident photons, whereas d denotes the film's thickness (measured either gravimetrically or interferometrically). Considering the reflection from the front film surface only (i.e., neglecting interference and multiple reflections) leads to the following formula for calculation of the spectral dependence of α[83]

$$\alpha(h\nu) = \frac{1}{d}\ln\frac{1 - R(h\nu)}{T(h\nu)} \quad (7)$$

where $R(h\nu)$ denotes the spectral dependence of the reflection coefficient. Equation 7 was slightly modified if also the reflection at the film−substrate interface was considered in the analyses of our experimental data, i.e.

$$\alpha(h\nu) = \frac{1}{d}\ln\frac{[1 - R(h\nu)]^2}{T(h\nu)} \quad (8)$$

In the most general case, that is, considering also multiple reflections within the film, we have calculated the spectral dependence of the absorption coefficient from the formula

$$T(h\nu) = \frac{[1 - R(h\nu)]^2\exp(-\alpha(h\nu)d)}{1 - R(h\nu)^2\exp(-2\alpha(h\nu)d)} \quad (9)$$

As we have found out in our present investigation, although the actual values of the absorption coefficient *are* affected upon inclusion of the effects due to reflection, the overall shape of the spectral dependence of α is not very sensitive to this. The last statement is particularly valid for the sub-band-gap spectral region, which is of central importance for the present study.

The spectral dependencies of the absorption coefficient of the nanocrystalline ZnSe films in the region of fundamental band-to-band electronic transitions for several temperatures within the range mentioned before are given in Figure 3.

In this study, we have actually focused on the lowest-energy direct band-to-band $\Gamma_8^v \rightarrow \Gamma_6^c$ transition from the absolute maximum of the valence band to the absolute minimum of the conduction band.[20,84−86] For more details concerning the bulk and quantized ZnSe band structure, the reader is referred to our previous publications.[63,64]

It is evident that, upon temperature lowering, the absorption onset is blue shifted, indicating a negative temperature coefficient of the band-gap energy. This point will be discussed in a quantitative manner further in this section. As can be seen, a qualitative characteristic of the functions $\alpha = f(h\nu)$ presented in Figure 3 is the absence of clearly defined excitonic peaks even at temperatures as low as 11 K. In the case of individual QDs, or diluted QD ensembles, such features are expected even at higher temperatures due to the evolution of energy bands into series of discretized electronic energy levels occurring as a result of the 3D confinement of charge carrier motions within a QD upon a crystal size decrease. In fact, such a property of individual QDs has been demonstrated in cases of colloidal QDs in solutions or in cases of diluted QD ensembles (where the dilution is achieved, for example, by appropriate capping ligand).[9−16] However, in the case of QD thin films synthesized by chemical methods, the nanoparticles are not monodispersed, but instead, the particle size distribution is rather wide. This point has been discussed in our previous publications.[55,56] Because of the quantum confinement effects occurring in the size range close to the Bohr excitonic radius of the material, the spectral dependence of the absorption coefficient is a rather complex function of the particle size distribution. If we denote the QD particle size probability distribution function (PDF) by $F(R)$, accounting only for the continuum DOS contribution to the absorption coefficient in the case of direct band-to-band transitions (i.e., neglecting the influence of electrostatic interaction between photogenerated charge carriers on the absorption process), the spectral dependence of the absorption coefficient may be represented by the following function:

$$\alpha(h\nu) = \frac{\int F(R)[A_0\sqrt{h\nu - E_g(R)}]\mathrm{d}R}{\int F(R)\mathrm{d}R} \quad (10)$$

In the previous equation, A_0 is a constant and the particle size distribution PDF is often described by either a Gaussian or a log-normal function, whereas $E_g(R)$ may be represented by some analytical model function, such as, for example, the one implied by the model of Brus, the hyperbolic band model, or Nosaka's model.[63] It is, therefore, obvious that the particle size distribution itself actually smears the excitonic absorption peaks, even if they are visible in single QDs. This is a situation frequently encountered in the case of QD thin films synthesized by chemical deposition methods. We will devote a separate study to the numerical modeling of the effects of the finite particle size distribution on the shape of the spectral dependence of α. Besides the previously outlined arguments, in the case of our films, however, ZnSe QDs are close-packed; that is, they form a continual thin film. When isolated QDs are brought in contact, the probability of interdot electronic coupling significantly increases and the effects related to this phenomenon are manifested. The most important overall consequence of the interdot electronic coupling is the formation of collective electronic states in an ensemble of quantum dots.[12,13,16,87−89] These states are delocalized within a finite number of nanocrystals of the 3D QD array. Although the exact mechanism of interdot coupling is still a subject of many debates in the literature, as it depends on the interdot distances and the particular material of which the dots are formed, in our case of QDs that are very closely packed (actually there is not an organic or capping layer between the dots), the tunneling mechanism is effectively responsible for charge carrier coupling phenomena. Therefore, it can be concluded that the interdot coupling mechanism (leading to formation of collective electronic states in 3D QD ensembles) could certainly further contribute to the observance of structureless absorption spectra in the studied 3D arrays of ZnSe QDs deposited as thin films. As the transitions to excitonic states could not be observed due to the outlined reasons, the further focus of our analysis was put on interband transition energies obtained by analysis of the semiconductor absorption functions and their temperature dependencies. Though, as mentioned before, the nonobservance of excitonic peaks in semiconductor QD films at room temperature has been well-documented and understood in terms of the QD size distribution (and also the interdot electron coupling when QDs are very small), to the best of our knowledge, this is the first experimental study that demonstrates that the excitonic transitions are not manifested at all in the optical absorption spectra of thin films composed of close-packed QDs *even at a temperature as low as 11 K*.

To get a deeper physical insight into the interband electronic transitions in nanocrystalline semiconductor films, the experimental absorption spectra were interpreted in the framework of the band theory of solid state,[5−8,20−22] but also accounting for the low-dimensional character of the studied systems, imposing a spatial confinement on the charge-carrier motions.[1−4]

In the case of a solid-state system, the band structure is actually a function of a three-dimensional wave vector ($\vec{k}$) within the Brillouin zone, which, on the other hand, corresponds to a Wigner−Zeits-type primitive unit cell of the reciprocal lattice (and is, therefore, dependent on the crystal structure). In the

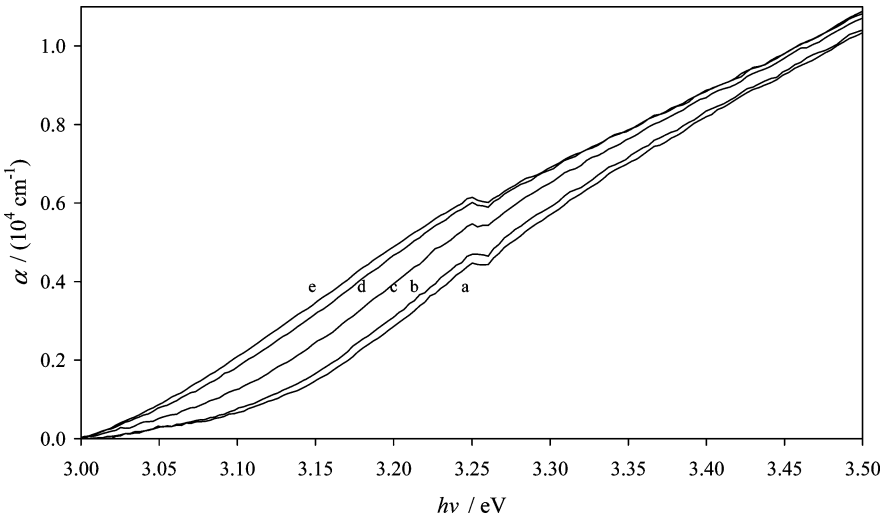

Figure 3. Spectral dependencies of the absorption coefficient of a nanostructured ZnSe thin film recorded at (a) 11, (b) 100, (c) 180, (d) 260, and (e) 340 K.

general case, the spectral dependence of the absorption coefficient is a complicated function, which involves many parameters related with the nature of the investigated system.[5−8,20−22,81] However, in a special case, when the investigated semiconductor is characterized with spherical symmetry of its energy bands, this relation could be rewritten in a simpler way in terms of the semiconductor absorption function

$$(\alpha(h\nu)h\nu)^n = \text{const.}(h\nu - E_g) \qquad (11)$$

where E_g denotes the band-gap energy of the investigated semiconducting system, whereas the exponent n depends on the type of electronic transitions. Such an approach is more useful in the course of interpretation of the obtained results. When a direct type of semiconductor is in question (the case in which the valence band absolute maximum and conduction band absolute minimum correspond to the same point of k-space), the interband transitions are not accompanied with a change of electronic momentum. Consequently, the exponent n can take two values, either 2 or 2/3. In the first case, electronic transitions are dipole-allowed, whereas in the second one, they are dipole-forbidden. Otherwise, when the considered semiconductor has an indirect band structure (valence band maximum and conduction band minimum correspond to different points in k-space), the interband transitions are accompanied with a change of electronic momentum. Because the laws of both conservation of energy and momentum have to be satisfied, indirect band-to-band electronic transitions necessary involve lattice phonons; that is, they are phonon-assisted. Lattice phonons have to be involved in the interband electronic transition in order to supply the necessary momentum. Their energetic contribution is negligible in comparison with E_g. In this case, the exponent n in eq 11 takes the value of 1/2 or 1/3 for dipole-allowed and dipole-forbidden indirect electronic transitions, respectively. In the context of getting a deeper physical insight into the nature of sub-band-gap absorption tails, it is worth pointing out that the considered equation of the form 11 does not take into account electrostatic interaction between photogenerated charge carriers.

Using the experimental data for spectral dependencies of the absorption coefficient for the synthesized nanocrystalline ZnSe thin films at various temperatures, we have constructed and analyzed the semiconductor absorption functions for all physically acceptable values of the exponent n. By a careful analysis of these functions, we concluded that the investigated system belongs to the group of semiconductors with a direct band structure. Therefore, the low-dimensional character of the deposited films does not affect the type of "interband" electronic transitions. The band-gap energies of the nanocrystalline films at various temperatures were determined by detailed analysis of the $(\alpha(h\nu)h\nu)^2 = f(h\nu)$ dependencies on the basis of a combined interpolation−extrapolation procedure. Having in mind that the dispersion relation does not follow a parabolic approximation (on which the previously considered form of the semiconductor absorption function is based) in the neighborhood of first Brillouin zone borders, linear least-squares fits of $(\alpha(h\nu)h\nu)^2 = f(h\nu)$ dependencies were carried out by successive inclusion or elimination of a number of neighboring points in the relevant energy range (wide enough), keeping in parallel an eye on the value of R^2. After that, extrapolating the linear dependencies to $(\alpha(h\nu)h\nu) = 0$, the band-gap energy for each temperature was calculated on the basis of the obtained correlation equations.

Note that the band-gap energy value of nanocrystalline ZnSe films at room temperature (and actually in the whole region of temperatures studied) is higher than the corresponding bulk value of 2.58 eV.[69] This is due to 3D confinement effects (i.e., size quantization effects). The charge carrier motions are confined in three spatial dimensions within the nanocrystals constituting the 3D QD array, which leads to a band-gap energy increase. This purely quantum effect is observable when the QD size is smaller than the excitonic Bohr radius for the corresponding bulk material. In our previous studies, we have analyzed and discussed in detail a number of issues related to size quantization effects in nanocrystalline ZnSe deposited in thin film form.[63,64] As mentioned before, to the best of our knowledge, this is the first study concerning the temperature dependence of the band-gap energy (and also of the sub-band-gap absorption tails) in size-quantized semiconductor nanocrystal arrays.

The temperature dependence of the band-gap energy of the synthesized nanocrystalline ZnSe films is shown in Figure 4. The experimental data for $E_g = f(T)$ were first fitted with a Varshni-type function[90] of the form (Figure 4a)

$$E_g(T) = E_g(0) - \alpha\frac{T^2}{T + T_0} \quad (12)$$

The Varshni coefficient α obtained from the least-squares fitting procedure is 8.2×10^{-4} eV K^{-1}. This value is almost twice larger than the one reported for bulk (macrocrystalline) zinc selenide (4.5×10^{-4} eV K^{-1}).[69] In Table 2, the values of all parameters obtained by fitting the experimental data to the Varshni function are compiled. Parameter T_0, which has often been found to be in close relation with the Debye temperature of the investigated material (in certain cases, almost equal to Θ_D), is nearly 399 K in the presently studied nanocrystalline QD array in thin film form. Such a value is in excellent agreement with the reported values of the Debye temperature for bulk ZnSe of 400 K.[69] However, the Varshni function is essentially an empirical one, based on the known behavior of the $E_g(T)$ dependence in various temperature regions. Although it is certainly quite useful for quantitative characterization of the $E_g(T)$ dependence, especially in the sense of determining the temperature coefficient of the band-gap energy and its comparison to the macrocrystalline value, further physical insight into the mechanisms responsible for the trend could not be obtained from this analysis. Note also that, similarly as reported in other studies,[27−33] besides the goodness of the overall fit (evident from Figure 4a), the Varshni-type function actually shows some deviations from the experimentally observed trend in the region of very low temperatures. To be able to get a further and deeper physical insight into the previously mentioned points, the experimental $E_g(T)$ data were also fitted to a Bose−Einstein-type function of the form[27−33]

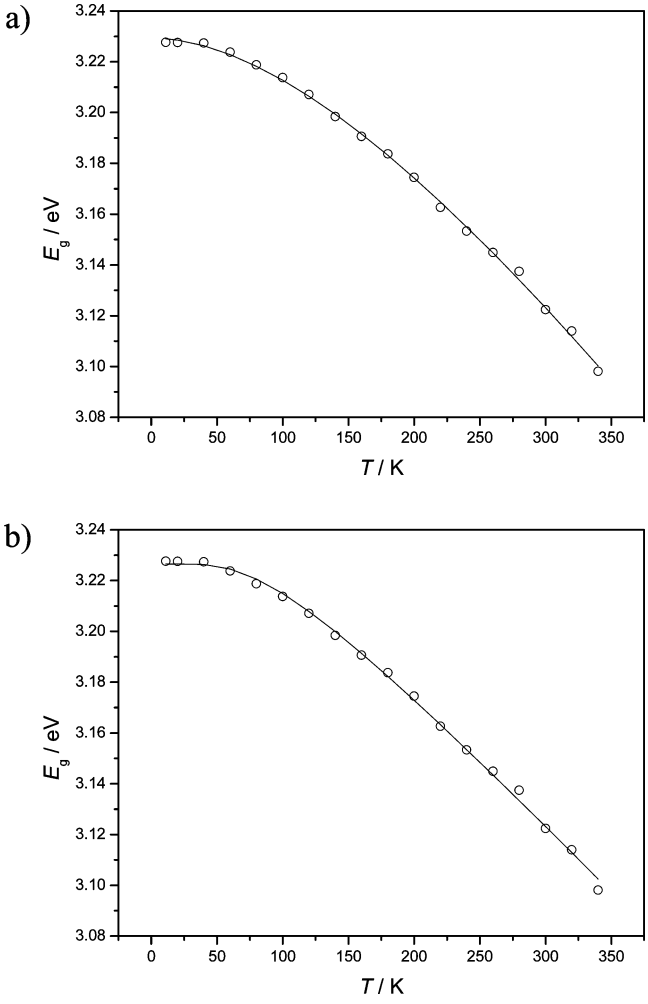

Figure 4. Temperature dependence of the band-gap energy of the synthesized nanocrystalline ZnSe films, fitted to a (a) Varshni-type function and the (b) Bose−Einstein function.

TABLE 2: Values of Parameters Obtained by Least-Squares Fitting of the Experimental $E_g = f(T)$ Data to the Varshni and Bose−Einstein Functions[a]

Varshni	$E_g(0)$/eV	α/(eV K^{-1})	T_0/K
	3.229	8.2×10^{-4}	398.8
Bose−Einstein	$E_g(0)$/eV	a_B/meV	Θ_E/K
	3.227	69.6	255.8

[a] See text for details.

$$E_g(T) = E_g(0) - \frac{2a_B}{\exp\left(\frac{\Theta_E}{T}\right) - 1} \quad (13)$$

Equation 13 has been derived considering the electron interaction with the phonon bath within the crystal. The parameter a_B is a measure of the electron−phonon interaction coupling within the crystal, whereas Θ_E is the average temperature of the phonons interacting with the electronic subsystem (i.e., The Einstein characteristic temperature for the investigated crystal). It could often be assumed that a Debye phonon spectrum with the Debye temperature Θ_D (related to Θ_E by the relation $\Theta_D = 4\Theta_E/3$) holds for an Einstein oscillator with a temperature Θ_E. Converting the Einstein temperature value obtained from the least-squares fit of the experimental data obtained in the present study (Figure 4b) to the Debye temperature, a value of 341 K is obtained for the last quantity (Table 2). This is in good agreement with the previously mentioned T_0 value obtained by fitting with the Varshni equation. The value of Varshni's parameter T_0 is actually somewhat higher than the estimated Θ_D value obtained from the Bose−Einstein fit, which is in line with the existing literature data for bulk semiconductors.[27−33] It has been clearly demonstrated, on the other hand, that the estimations of the Debye temperature for a given material on the basis of a Varshni-type equation give too high values, especially in the case of polar semiconductors.[27−33] If we, therefore, accept the value of ∼340 K for the Debye temperature of the presently studied ZnSe nanocrystalline array, this value is obviously lower than that reported for bulk ZnSe (400 K[69]). Comparing the presently obtained values with those characteristic of a macrocrystalline ZnSe indicates a certain decrease of the Debye temperature for the title material upon a crystal size decrease (for about 15%). We attribute this finding to the following. Analogously as the crystal size reduction exhibits 3D confinement effects on the charge carrier motions within the zero-dimensional nanocrystals, which results in a significant band-gap blue shift, such spatial confinement is also exerted on the phonon system in the studied semiconductor.[91−97] It has been shown both experimentally and by theoretical modeling that the lattice modes exhibit a frequency downshift upon a particle size decrease. Actually, the positions and half-widths of bands due to the TO and LO modes of a particular semiconductor QD, appearing, for example, in the Raman spectra of such low-dimensional systems, could even be used to derive conclusions concerning the nanocrystal sizes and size distributions.[91−97] Because the Debye temperature is actually proportional to the energy of oscillators constituting the system

($\Theta_D = \hbar\omega_{max}/k_B$, where ω_{max} corresponds to the maximum vibrational frequency in the Debye model), a shift of the lattice vibrations to a lower frequency upon a particle size decrease would, in fact, be expected to lead to lower values of Θ_D. For example, in the case of Si nanocrystals, the Raman shifts due to confinement effects could be described by the following confinement model equation[97]

$$\omega(L) = \omega_0 - A\left(\frac{a}{L}\right)^{\gamma} \tag{14}$$

where $\omega(L)$ is the frequency of a Raman phonon in a nanocrystal with size L, ω_0 is the frequency of an optical phonon at the Brillouin zone center, and a is the lattice constant, whereas A and γ are model parameters employed to describe the vibrational confinement due to the finite size within the semiconductor nanocrystal. Concerning the title material, also, certain shifts of the LO and TO mode positions have been detected by Raman spectroscopy. Thus, it has been reported in ref 91 that the LO and TO modes in the case of macroscrystalline intrinsic ZnSe appear at about 251 and 207 cm^{-1}. On the other hand, in a recent study devoted to ZnSe nanocrystals diluted in polyvinyl alcohol (PVA),[94] it has been shown that the LO mode is red shifted compared with the bulk value and the corresponding band in the Raman spectra appears in the spectral region from 239 to 234 cm^{-1}, depending on the actual nanocrystal size. Another proof for the red shift of the confined LO modes in the case of ZnSe−ZnTe superlattices with respect to the bulk value has been given in ref 93 and also in ref 98, where lattice vibrations in alternating monolayers of ZnSe and ZnTe have been considered.

Also, the characteristic Einstein temperature obtained by fitting the experimental data to eq 12 corresponds to a phonon frequency of about 177.5 cm^{-1}, which is lower than both the LO and the TO mode frequencies of bulk ZnSe, in line with the previous discussion and the outlined arguments.

To the best of our knowledge, the present paper is the first work in which it has been demonstrated that the Debye temperature of a QD solid has been lowered in comparison with the bulk analogue.

3.3. Urbach−Martienssen Absorption Tails in the Optical Spectra of As-Deposited ZnSe Quantum Dots in Thin Film Form and Their Temperature Dependence. As mentioned in the Introduction, much attention has been paid in the literature to the existence of exponential absorption tails for sub-band-gap photon energies in the case of both macrocrystalline and amorphous semiconducting and isolating materials (usually known as Urbach−Martienssen (UM) tails). However, there is practically a lack of such data when semiconducting nanocrystalline materials are in question. The existence of UM tails has been shown to be of a quite universal nature in semiconductors and isolators, aside from the various theoretical explanations provided in the literature for this type of behavior. Various mechanisms have been proposed in the literature, which could be involved in this type of absorption phenomena, but usually, two effects have been given the main emphasis, both of which are related to the interaction of excitons with the optical phonons.[20] The first effect considered is connected to the momentary localization of the excitons in the randomly fluctuating field of the optical phonons, whereas the second one is the ionization of their electric field. Expressing the UM absorption in a quantitative manner, for the range of energies $E < E_g$, the optical absorption coefficient of a semiconductor shows a temperature-dependent exponential tail of the form

$$\alpha(E,T) = \alpha_0 \cdot \exp\left(\frac{E - E_0}{E_U(T,X)}\right) \tag{15}$$

In the last equation, α_0 and E_0 are constants, which can be determined from the dependencies of $\ln(\alpha)$ on E measured at series of different temperatures. E_0 nearly coincides with the energy of the lowest free exciton state at zero lattice temperature. The term E_U from the exponential function, determining the steepness of the Urbach tail, is the Urbach energy. This parameter is a rather important characteristic of a given semiconducting material. It is a function of temperature and the degree of structural disorder of the studied material. Following the model proposed by Cody,[99] the dependence of E_U on temperature can be expressed by the following equation

$$E_U(T,X) = \frac{E_p}{2\sigma_0} \cdot \left[X + \coth\left(\frac{E_p}{2kT}\right)\right] \tag{16}$$

where E_p is the phonon energy, σ_0 is a material-dependent parameter (usually of the order of unity), and k is the Boltzmann constant, whereas X is a parameter that is a measure of the degree of structural disorder of the material in question. In a quantitative manner, X is defined by the ratio of the mean square deviation of atomic position caused by the actual structural disorder, $\langle U_x^2 \rangle$, to the zero-point uncertainty in the atomic positions, $\langle U^2 \rangle_0$, i.e.

$$X = \frac{\langle U_x^2 \rangle}{\langle U^2 \rangle_0} \tag{17}$$

Equation 16 is, in fact, an extension of the original models of Urbach and Martienssen in which the parameter X was set to 0. As shown by Cody and co-workers,[99] and also by Yang et al.,[100] besides the thermal component to the structural disorder (reflecting in the temperature-dependent width of the exponential tail), there is an additional, that is, nonthermal, component to the disorder, which is clearly manifested especially in the case of amorphous semiconductors. This contribution is expected to exhibit a temperature-independent component to the Urbach exponential absorption edge. The previous statements imply that the Urbach energy can be split into two contributions—a temperature-dependent and a temperature-independent term:

$$E_U(T,X) = E_U(T) + E_U(X) \tag{18}$$

The temperature-dependent term is related to the thermal disorder of the material, whereas the temperature-independent contribution reflects its inherent structural disorder. In the paper by Cody and co-workers,[99] the following explicit equation of the form 18 has been proposed

$$E_U(T,X) = \frac{\Theta_E}{\sigma_0} \cdot \left[\frac{1+X}{2} + \frac{1}{\exp(\Theta_E/T) - 1}\right] \tag{19}$$

where σ_0 is the Urbach edge parameter, which will be addressed in some more detail further in the article. Yang et al.[100] suggested the following generalized form of eq 18 for analysis of experimental data

$$E_U(T,X) = [E_U(T) + E_U(X)] = A\left[\frac{1}{\exp(\Theta_E/T) - 1}\right] + B \quad (20)$$

where only the first term is temperature-dependent. The last equation could be derived by modeling the temperature dependence of E_U by the concept of an Einstein oscillator, taking into account the contributions of dynamical thermal, as well as static structural, and compositional disorders in the sample. Actually, the first term in eq 20 represents the contribution of electron/exciton−phonon interaction, such as the Debye−Waller factor, and the second term is due to the mean-square deviation of atomic positions from a perfectly ordered lattice, caused by the structural disorder.

A plot of ln(α) versus $h\nu$ just below the absorption edge for the investigated ZnSe nanocrystalline films in the studied temperature region is given in Figure 5. This plot clearly demonstrates the validity of the Urbach−Martienssen rule for 3D QD assemblies deposited in thin film form. The calculated Urbach energies are plotted versus temperature in Figure 6, together with the interpolating function of the form 20. As can be seen, the fit to experimental data is excellent. The parameters A and B in eq 20 obtained by the least-squares fitting procedure are given in Table 3. It could be concluded from the data presented so far that the values of Urbach energies in the presently studied system are larger than the values measured for other systems with a less pronounced (or not pronounced at all) nanocrystalline character.[25,26] As follows from the model of Cody, such high values of Urbach energies are due to the relatively high degree of structural disorder in the 3D QD arrays. It could be concluded from Table 3 that the dynamical thermal term in eq 20 accounts only for less than 14% in the overall Urbach energy values. It, therefore, follows that it is the intrinsic degree of structural disorder in the studied nanocrystalline arrays (i.e., the nonthermal contribution) that governs the overall E_U value. As shown by our recent investigations, for example, the Urbach energies in the case of semiconducting cadmium selenide quantum dots deposited in thin film form by our group are also of the order of magnitude of 100−200 meV.[101] Note, however, that, besides on the degree of structural disorder, the exact values of the Urbach energies for particular materials also depend on other material-dependent parameters (eq 16), such as σ_0 and the phonon energy E_p. Also, even for one and the same material, the Urbach energy varies even in the case of crystals characterized with the same average size but obtained by different chemical methods.[35−42] It is worth noting, however, that such high values for the Urbach energies (i.e., Urbach tails with large widths) have been already found for particular materials, mostly with an amorphous or partially crystalline character.[44−53] It could be, therefore, concluded that nanocrystalline thin films behave similarly as amorphous materials in this respect. To the best of our knowledge, however, this is the first experimental study in which the validity of the Urbach−Martienssen rule in the case of nanocrystalline thin films has been demonstrated.

Another prediction of the model of Cody[99] concerns the relation between the band-gap energy and the Urbach energy. It follows from this model that the functional dependence of E_g on E_U should be linear, expressed by the following equation

$$E_g(T,X) = E_g(0,0) - \langle U^2\rangle_0 D\left(\frac{E_U(T,X)}{E_U(0,0)} - 1\right) \quad (21)$$

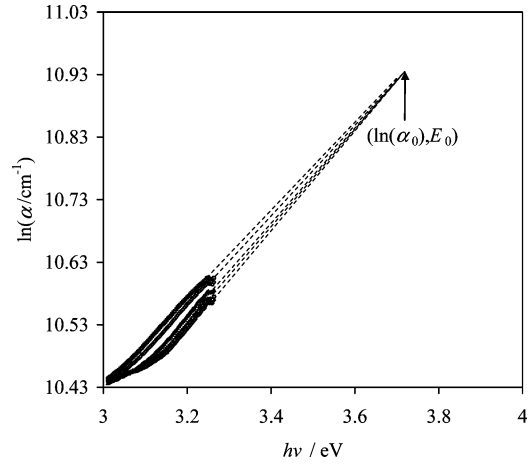

Figure 5. Plot of ln(α) vs $h\nu$ just below the absorption edge for the investigated ZnSe nanocrystalline films in the studied temperature region, demonstrating the validity of the Urbach rule.

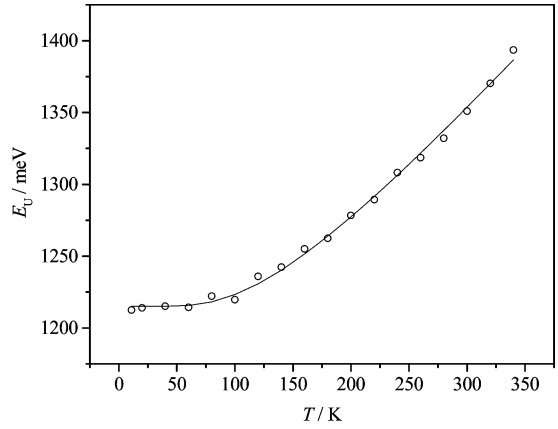

Figure 6. Plot of the calculated Urbach energies vs temperature, together with a fit to the function proposed by Yang et al.

TABLE 3: Values of Parameters Obtained by Least-Squares Fitting of the Experimental $E_U = f(T)$ Data to the Function Proposed by Yang et al.[a]

A/meV	B/meV	Θ_E/K
191.9	1208.9	255.8

[a] See text for details.

where $E_g(0,0)$ and $E_U(0,0)$ are the band-gap energy and Urbach energy at a temperature of absolute zero for a material lacking any structural disorder ($X = 0$), whereas D is a second-order deformation potential; correspondingly, $E_g(T, X)$ and $E_U(T, X)$ are the band-gap energy and Urbach energy at finite temperature for a material with a finite degree of structural disorder. The linear relationship between E_g and E_U has been demonstrated for various materials with varying degrees of structural disorder.[99] However, to the best of our knowledge, its applicability has not been tested in the case of nanostructured thin films. In Figure 7, a plot of the measured E_g versus the calculated E_U values is given, together with a linear least-squares fit of the experimental data. It could be clearly seen that the observed dependence is fairly linear, and therefore, the model of Cody works in this respect in the case of nanocrystalline films as well.

An alternative variant of eq 15, which has also been often used to express the dependence of α on the photon energy in the sub-band-gap region, has the form[27−33]

$$\alpha(E, T) = \alpha_0 \exp\left(\frac{\sigma(T)}{kT}(E - E_0)\right) \quad (22)$$

where σ is a steepness parameter and T is the thermodynamic temperature, whereas k is the Boltzmann constant. Within this notation, the Urbach energy E_U is inversely proportional to the steepness parameter σ, i.e.

$$E_U = \frac{kT}{\sigma} \quad (23)$$

The temperature dependence of the steepness parameter σ has often been expressed by the following relation in the literature:[27−33]

$$\sigma(T) = \sigma_0\left(\frac{2kT}{h\nu_p}\right)\tanh\left(\frac{h\nu_p}{2kT}\right) \quad (24)$$

In the last equation, the parameter σ_0 (which is temperature-independent but material-dependent) is inversely proportional to the strength of the coupling between electrons/excitons and phonons, whereas $h\nu_p$ is the average energy of phonons contributing to the UM tails. The last equation, therefore, implies that, from the studies of the temperature dependence of the UM tails, certain information about the interaction of electrons/excitons with phonons in semiconductors could be obtained. A plot of σ versus T constructed on the basis of our experimental data is presented in Figure 8 together with the interpolation function of the form 24. It could be clearly seen that the fit to experimental data is excellent. The parameters σ_0 and $h\nu_p$ obtained from the least-squares fit to the experimental data are 0.033 and 81.2 meV, the last one corresponding to a phonon frequency value of 653.5 cm^{-1}. As compared with the positions of LO or TO phonon modes in the Raman spectra of ZnSe (discussed before), such a value is significantly higher. However, higher values of average phonon frequencies contributing to the UM tails have actually been reported in the case of various systems (though not of a nanocrystalline nature).[102−108] For example, in II−VI type of semiconductors with a zincblende structural type, higher values of $h\nu_p$ than the LO phonon energies have been attributed to higher crystal symmetry.[107,108] In some other systems, however, such as ternary compounds, mixed chalcogenides, etc., they were attributed to structural disorders (e.g., cation−cation disorder, cation vacancies, and interstitials, even deviations from ideal stoichiometry).[102−106] Because, as discussed before, analyses of the current results within the framework of the model of Cody and related approaches strongly imply a relatively high level of structural disorder in the 3D QD arrays considered in the present study, this could be certainly the main reason for the discussed results.

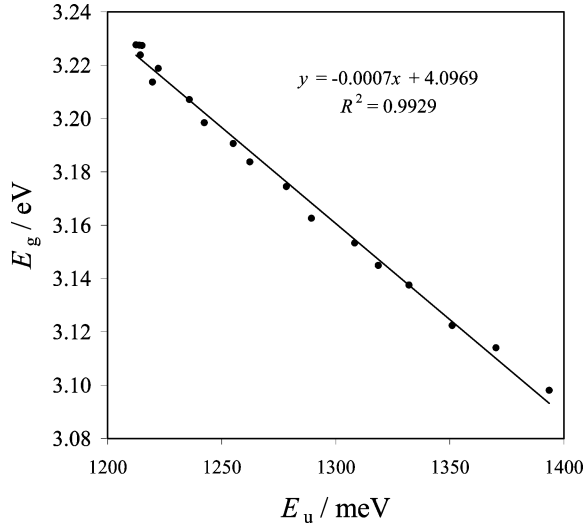

Figure 7. Plot of the measured E_g vs the calculated E_U values for the studied material, together with a linear least-squares fit.

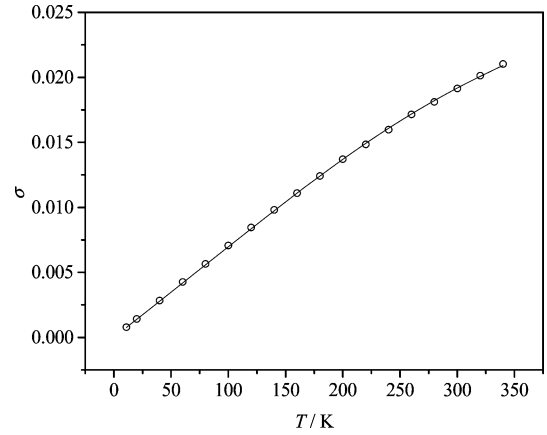

Figure 8. Plot of σ vs T constructed on the basis of temperature-dependent optical spectroscopy data.

4. Conclusions

In the present paper, we have studied the temperature dependence of the band-gap energy and the sub-band-gap absorption tails in 3D assemblies of close-packed strongly quantized ZnSe QDs deposited in the form of thin films. This is the first study of this type in the literature concerning 3D QD arrays. The most important insights from the study may be summarized as follows:

The experimentally measured temperature dependence of the band-gap energy of the films could be excellently fitted with both Varshni-type and Bose−Einstein-type functions. The temperature coefficient of the band-gap energy in the strongly quantized QD thin films is almost twice larger than the corresponding value characteristic for bulk ZnSe. The Debye temperature of the studied QD solid was found to be lower than that of the corresponding bulk material. The last finding was attributed to the phonon confinement effects.

The Urbach rule was found to hold for the 3D QD assemblies deposited in thin film form. Because of the relatively high degree of structural disorder in the QD solids, the values of Urbach energies are much higher than those usually found in macrocrystalline semiconductors. Concerning these quantities, the QD solids are, therefore, similar to amorphous materials.

The temperature dependence of the Urbach energy could be excellently fitted to a Cody or Yang-type function. In contrast to macrocrystalline semiconductors, the dynamical thermal (temperature-dependent) contribution to E_U, in the framework of Cody's and similar models, was found to account only for less than 15% in the overall Urbach energy values in the investigated 3D QD arrays. This was attributed to the very high degree of inherent structural disorder in the QD arrays.

In accordance with the predictions of Cody's model, an excellent linear correlation was found between the Urbach energies and band-gap energies of the studied materials.

Analyses of the temperature dependence of the steepness parameter of the sub-band-gap absorption tail σ imply a rather

high energy of the phonons contributing to the Urbach−Martienssen tails in the optical absorption of the QD arrays.

Acknowledgment. This work has been partially supported by the Bulgarian Ministry of Education and Science under Grant BM-1 and by the Macedonian Ministry of Education and Science under bilateral Bulgarian-Macedonian Project BM-1.

References and Notes

(1) Collier, C. P.; Vossmeyer, T.; Heath, J. R. *Annu. Rev. Phys. Chem.* **1998**, *49*, 371.
(2) Yoffe, A. D. *Adv. Phys.* **2001**, *50*, 1.
(3) Yoffe, A. D. *Adv. Phys.* **2002**, *51*, 799.
(4) Landman, U.; Luedtke, W. D. *Faraday Discuss.* **2004**, *125*, 1.
(5) Yu, P. Y.; Cardona, M. *Fundamentals of Semiconductors*; Springer: Berlin, 1999.
(6) Seeger, K. *Semiconductor Physics*; Springer-Verlag: New York, 1997.
(7) Dalven, R. *Introduction to Applied Solid State Physics*; Plenum Press: New York, 1990.
(8) Callister, W. D. *Materials Science and Engineering*; Wiley: New York, 1997.
(9) Kagan, C. R.; Murray, C. B.; Nirmal, M.; Bawendi, M. G. *Phys. Rev. Lett.* **1996**, *76*, 1517.
(10) Kagan, C. R.; Murray, C. B.; Bawendi, M. G. *Phys. Rev. B* **1996**, *54*, 8633.
(11) Gindele, F.; Westphäling, R.; Woggon, U.; Spanhel, L.; Ptatschek, V. *Appl. Phys. Lett.* **1997**, *71*, 2181.
(12) Artemyev, M. V.; Bibik, A. I.; Gurinovich, L. I.; Gaponenko, S. V.; Woggon, U. *Phys. Rev. B* **1999**, *60*, 1504.
(13) Artemyev, M. V.; Woggon, U.; Jaschinski, H.; Gurinovich, L. I.; Gaponenko, S. V. *J. Phys. Chem. B* **2000**, *104*, 11617.
(14) Artemyev, M. V.; Bibik, A. I.; Gurinovich, L. I.; Gaponenko, S. V.; Jaschinski, H.; Woggon, U. *Phys. Status Solidi B* **2001**, *224*, 393.
(15) Kim, B. S.; Islam, M. A.; Brus, L. E.; Herman, I. P. *J. Appl. Phys.* **2001**, *89*, 8127.
(16) Kim, D. E.; Islam, M. A.; Avila, L.; Herman, I. P. *J. Phys. Chem. B* **2003**, *107*, 6318.
(17) Urbach, F. *Phys. Rev.* **1953**, *92*, 1324.
(18) Martienssen, W. *J. Phys. Chem. Solids* **1957**, *2*, 257.
(19) Cody, G. D.; Tiedje, T.; Abeles, B.; Brooks, B.; Goldstein, Y. *Phys. Rev. Lett.* **1981**, *47*, 1480.
(20) Klingshirn, C. F. *Semiconductor Optics*; Springer-Verlag: Berlin, 1997.
(21) Seeger, K. *Semiconductor Physics*; Springer-Verlag Wien: New York, 1973.
(22) Ashcroft, N. W.; Mermin, N. D. *Solid State Physics*; Holt, Rinehart and Winston: New York, 1976.
(23) Ohring, M. *The Materials Science of Thin Films*; Academic Press: San Diego, CA, 1992.
(24) Memming, R. *Semiconductor Electrochemistry*; Wiley-VCH: Weinheim, Germany, 2001.
(25) Rakhshani, A. E.; Al-Azab, A. S. *J. Phys.:Condens. Matter* **2000**, *12*, 5746.
(26) Rakhshani, A. E. *J. Phys.:Condens. Matter* **2000**, *12*, 4391.
(27) Abay, B.; Güder, H. S.; Efeoğlu, H.; Yoğurtçu, Y. K. *Semicond. Sci. Technol.* **2000**, *15*, 535.
(28) Abay, B.; Güder, H. S.; Efeoğlu, H.; Yoğurtçu, Y. K. *J. Phys. Chem. Solids* **2001**, *62*, 747.
(29) Abay, B.; Güder, H.; Yoğurtçu, Y. K. *Solid State Commun.* **1999**, *112*, 489.
(30) Abay, B.; Güder, H. S.; Efeoğlu, H.; Yoğurtçu, Y. K. *Physica B* **1998**, *254*, 148.
(31) Abay, B.; Güder, H. S.; Efeoğlu, H.; Yoğurtçu, Y. K. *Phys. Status Solidi B* **2001**, *227*, 469.
(32) Abay, B.; Güder, H. S.; Efeoğlu, H.; Yoğurtçu, Y. K. *J. Phys. D: Appl. Phys.* **1999**, *32*, 2942.
(33) Abay, B.; Güder, H. S.; Efeoğlu, H.; Yoğurtçu, Y. K. *J. Appl. Phys.* **1998**, *84*, 3872.
(34) Ate, A.; Gürbulak, B.; Yldrm, M.; Doan, S. *Physica E* **2003**, *16*, 274.
(35) Meeder, A.; Fuertes Marróna, D.; Chub, V.; Condec, J. P.; Jäger-Waldaud, A.; Rumberga, A.; Lux-Steinera, M. Ch. *Thin Solid Films* **2002**, *403−404*, 495.
(36) Studenyak, I. P.; Kranjec, M.; Kovács, Gy. Sh.; Panko, V. V.; Mitrovcij, V. V.; Mikajlo, O. A. *Mater. Sci. Eng., B* **2003**, *97*, 34.
(37) Studenyak, I. P.; Kranjec, M.; Kovács, Gy. Sh.; Desnica-Frankovic, I. D.; Molnar, A. A.; Panko, V. V.; Slivka, V.; Yu, *J. Phys. Chem. Solids* **2002**, *63*, 267.
(38) Vijaya Prakash, G.; Narayana Rao, D.; Bhatnagar, A. K. *Solid State Commun.* **2001**, *119*, 39.
(39) Studenyak, I. P.; Kranjec, M.; Kovács, Gy. S.; Pan'ko, V. V.; Desnica, I. D.; Slivka, A. G.; Guranicha, P. P. *J. Phys. Chem. Solids* **1999**, *60*, 1897.
(40) Kranjec, M.; Desnica, I. D.; Studenyak, I. P.; Kovacs, Gy. Sh.; Potory, M. V.; Voroshilov, Yu, V.; Gebesh, V. Yu. *Mater. Res. Bull.* **1999**, *34*, 2297.
(41) Mullins, J. T.; Huntley, D. M.; Aylmore, R. C.; Brinkman, A. W. *J. Cryst. Growth* **1998**, *184−185*, 1114.
(42) Kranjec, M.; Studenyak, I. P.; Bilanchuk, V. V.; Dyordyay, V. S.; Panko, V. V. *J. Phys. Chem. Solids* **2004**, *65*, 1015.
(43) Saitoh, A.; Komatsu, T.; Karasawa, T. *J. Lumin.* **2000**, *87−89*, 633.
(44) Weinstein, I. A.; Zatsepin, A. F.; Kortov, V. S. *J. Non-Cryst. Solids* **2001**, *279*, 77.
(45) Nakata, H.; Murayama, K.; Miyazaki, S.; Hirose, M. *J. Non-Cryst. Solids* **2000**, *266−269*, 1067.
(46) Tews, R.; Suchaneck, G.; Kottwitz, A.; Abramov, A. S.; Kosarev, A. I. *J. Non-Cryst. Solids* **1998**, *227−230*, 478.
(47) Fritze, M.; Kastalsky, A.; Cunningham, J. E.; Knox, W. H.; Pathak, R. N.; Perakis, I. E. *Solid State Commun.* **1996**, *100*, 497.
(48) Jarzbek, B.; Weszka, J.; Burian, A.; Pocztowski, G. *Thin Solid Films* **1996**, *279*, 204.
(49) Coulibaly, S. P.; De Chelle, F.; Berger, J. M.; Ferraton, J. P.; Donnadieu, A.; Magariño, J.; Kaplan, D. *Thin Solid Films* **1984**, *115*, 263.
(50) Lin, S.; Feldman, B. J. *Solid State Commun.* **1991**, *80*, 371.
(51) Melsheimer, J.; Ziegler, D. *Thin Solid Films* **1985**, *129*, 35.
(52) Grein, C. H.; John, S. *Solid State Commun.* **1989**, *70*, 87.
(53) Berger, J. M.; de Chelle, F.; Ferraton, J. P.; Donnadieu, A. *Thin Solid Films* **1983**, *105*, 107.
(54) Pejova, B.; Tanuševski, A. *J. Phys. Chem. C* **2008**, *112*, 3525.
(55) Pejova, B.; Grozdanov, I.; Nesheva, D.; Petrova, A. *Chem. Mater.* **2008**, *20*, 2551.
(56) Nesheva, D.; Aneva, Z.; Pejova, B.; Grozdanov, I.; Petrova, A. *J. Optoelectron. Adv. Mater.* **2009**, *11*, 1347.
(57) Pejova, B. *J. Solid State Chem.* **2008**, *181*, 1961.
(58) Pejova, B. *Mater. Res. Bull.* **2008**, *43*, 2887.
(59) Pejova, B.; Grozdanov, I. *Thin Solid Films* **2007**, *515*, 5203.
(60) Pejova, B.; Grozdanov, I. *Mater. Chem. Phys.* **2006**, *99*, 39.
(61) Pejova, B.; Tanuševski, A.; Grozdanov, I. *J. Solid State Chem.* **2006**, *178*, 1786.
(62) Pejova, B.; Grozdanov, I. *Czech. J. Phys.* **2006**, *56*, 75.
(63) Pejova, B.; Grozdanov, I. *Mater. Chem. Phys.* **2005**, *90*, 35.
(64) Pejova, B.; Tanuševski, A.; Grozdanov, I. *J. Solid State Chem.* **2004**, *177*, 4785.
(65) Pejova, B.; Grozdanov, I. *Mater. Lett.* **2004**, *58*, 666.
(66) Pejova, B.; Tanuševski, A.; Grozdanov, I. *J. Solid State Chem.* **2003**, *174*, 276.
(67) Pejova, B.; Tanuševski, A.; Grozdanov, I. *J. Solid State Chem.* **2003**, *172*, 381.
(68) Pramanik, P.; Biswas, S. *J. Electrochem. Soc.* **1986**, *133*, 350.
(69) Novoselova, A. B., Ed. *Physical and Chemical Properties of Semiconductors*; Moscow, 1978.
(70) Empedocles, S. A.; Norris, D. J.; Bawendi, M. G. *Phys. Rev. Lett.* **1996**, *77*, 3873.
(71) Kim, C. C.; Sivananthan, S. *Phys. Rev. B* **1996**, *53*, 1475.
(72) Ohtake, Y.; Okamoto, T.; Yamada, A.; Kongai, M.; Saito, K. *Sol. Energy Mater. Sol. Cells* **1997**, *49*, 269.
(73) Turner, A. K.; Woodcock, J. M.; Özsan, M. E. *Sol. Energy Mater. Sol. Cells* **1994**, *35*, 263.
(74) Pejova, B.; Grozdanov, I. *J. Solid State Chem.* **2001**, *158*, 49.
(75) *Microsoft EXCEL*; Microsoft Corporation, 2003.
(76) *MICROCAL ORIGIN*, version 5.0; Microcal Software, Inc., 1991−1997.
(77) Adachi, S. *Phys. Rev. B* **1991**, *12*, 9569.
(78) Gorer, S.; Hodes, G. *J. Phys. Chem.* **1994**, *98*, 5338.
(79) Weller, M. T. *Inorganic Materials Chemistry*; Oxford University Press: Oxford, U.K., 1997.
(80) JCPDS; International Center for Diffraction Data, No. 37-1463.
(81) Pejova, B. In *Progress in Solid State Chemistry Research*; Buckley, R. W., Ed.; Nova Science Publishers: New York, 2007.
(82) Stokes, A. R. In *X-Ray Diffraction by Polycrystalline Materials*; Peiser, H. S., et al., Eds.; Chapman & Hall: London, 1960.
(83) Pankove, J. I. *Optical Processes in Semiconductors*; Prentice-Hall: Englewood Cliffs, NJ, 1971.
(84) Adachi, S. *Phys. Rev. B* **1991**, *12*, 9569.
(85) Chestnoy, N.; Hull, R.; Brus, L. E. *J. Chem. Phys.* **1986**, *85*, 2237.
(86) Baldereschi, A.; Lipari, N. G. *Phys. Rev. B* **1971**, *3*, 439.
(87) Artemyev, M. V.; Bibik, A. I.; Gurinovich, L. I.; Gaponenko, S. V.; Jaschinski, H.; Woggon, U. *Phys. Status Solidi B* **2001**, *224*, 393.
(88) Micic, O. I.; Ahrenkiel, S. P.; Nozik, A. J. *Appl. Phys. Lett.* **2001**, *78*, 4022.

(89) Kim, B. S.; Avila, L.; Brus, L. E.; Herman, I. P. *Appl. Phys. Lett.* **2000**, *76*, 3715.
(90) Varshni, Y. P. *Physica* **1967**, *34*, 149.
(91) Rai, B. K.; Katiyar, R. S.; Chen, K.-T.; Burger, A. *J. Appl. Phys.* **1998**, *83*, 6011.
(92) Bauer, S.; Berger, H.; Link, P.; Gebhardt, W. *J. Appl. Phys.* **1993**, *74*, 3916.
(93) Cui, J.; Wang, H.; Gan, F.; Li, A. *J. Cryst. Growth* **1991**, *111*, 811.
(94) Badr, Y.; Mahmoud, M. A. *Spectrochim. Acta A* **2006**, *65*, 584.
(95) Richter, H.; Wang, Z. P.; Ley, L. *Solid State Commun.* **1981**, *39*, 625.
(96) Iqbal, Z.; Vepøek, S. *J. Phys. C: Solid State Phys.* **1982**, *15*, 377.
(97) Zi, J.; Büscher, H.; Falter, C.; Ludwig, W.; Zhang, K.; Xie, X. *Appl. Phys. Lett.* **1996**, *69*, 200.
(98) Takemura, Y.; Kakuno, K.; Yamada, A.; Konagai, M. *Appl. Phys. Lett.* **1993**, *63*, 3176.
(99) Cody, G. D.; Tiedje, T.; Abeles, B.; Brooks, B.; Goldstein, Y. *Phys. Rev. Lett.* **1981**, *47*, 1480.
(100) Yang, Z.; Homewood, K. P.; Finney, M. S.; Harry, M. A.; Reeson, K. J. *J. Appl. Phys.* **1995**, *78*, 1958.
(101) Pejova, B.; Abay, B.; Grozdanov, I.; Yoğurtçu, Y. K. Manuscript in preparation.
(102) Shioda, T.; Chichibu, S.; Irie, T.; Nakanishi, H.; Kariya, T. *J. Appl. Phys.* **1996**, *80*, 1106.
(103) Medvedkin, G. A.; Rud, Y. V.; Tairov, M. A. *Phys. Status Solidi B* **1987**, *144*, 809.
(104) Wasim, S. M.; Marin, G.; Rincón, C.; Sánchez Pérez, G.; Mora, A. E. *J. Appl. Phys.* **1998**, *83*, 3318.
(105) Wasim, S. M.; Marin, G.; Rincón, C.; Sánchez Pérez, G.; Mora, A. E. *J. Appl. Phys.* **1998**, *84*, 5823.
(106) Wasim, S. M.; Marin, G.; Rincón, C.; Sánchez Pérez, G.; Bocaranda, P.; Mora, A. E. *J. Phys. Chem. Solids* **2000**, *61*, 669.
(107) Kranjcec, M.; Desnica, D. I.; Čelustka, B.; Kovacs, Gy. Sh.; Studenyak, I. P. *Phys. Status Solidi A* **1994**, *144*, 223.
(108) Desnica, D. I.; Kranjcec, M.; Čelustka, B. *J. Phys. Chem. Solids* **1991**, *52*, 915.

JP102773Z